Available online at www.sciencedirect.com
ScienceDirect
Journal of Power Sources 177 (2008) 40–49
JOURNAL OF POWER SOURCES
www.elsevier.com/locate/jpowsour

Electrochemical performance of an air-breathing direct methanol fuel cell using poly(vinyl alcohol)/hydroxyapatite composite polymer membrane

Chun-Chen Yang *, Shwu-Jer Chiu, Che-Tseng Lin

Department of Chemical Engineering, Mingchi University of Technology, Taipei Hsien 243, Taiwan, ROC

Received 29 September 2007; accepted 4 November 2007
Available online 12 November 2007

Abstract

A novel composite polymer membrane based on poly(vinyl alcohol)/hydroxyapatite (PVA/HAP) was successfully prepared by a solution casting method. The characteristic properties of the PVA/HAP composite polymer membranes were examined by thermal gravimetric analysis (TGA), X-ray diffraction (XRD), scanning electron microscopy (SEM), micro-Raman spectroscopy and AC impedance method. An air-breathing DMFC, comprised of an air cathode electrode with MnO_2/BP2000 carbon inks on Ni-foam, an anode electrode with PtRu black on Ti-mesh, and the PVA/HAP composite polymer membrane, was assembled and studied. It was found that this alkaline DMFC showed an improved electrochemical performance at ambient temperature and pressure; the maximum peak power density of an air-breathing DMFC in 8 M KOH + 2 M CH_3OH solution is about 11.48 mW cm^{-2}. From the application point of view, these composite polymer membranes show a high potential for the DMFC applications.

Keywords: Composite polymer membrane; Poly(vinyl alcohol) (PVA); Hydroxyapatite (HAP); Direct methanol fuel cell (DMFC); Alkaline; MnO_2

1. Introduction

Direct methanol fuel cells (DMFCs) [1–43] have recently received a lot of attentions due to their high-energy density (6100 W h kg^{-1}) and low emission of pollutants. The DMFC has attracted much attention because of its use of liquid methanol fuel, which is easy to deliver and store. More importantly, liquid fuel can be used at ambient temperature and pressure, which makes the DMFC easy to use with portable 3C electronic devices [13–18].

However, the development of acidic DMFC has faced several serious problems: (i) slow methanol oxidation kinetics, (ii) the poisoning of CO intermediate on the Pt surface, (iii) the high methanol crossover through the polymer membrane, (iv) the high costs of the Nafion membrane and Pt catalyst.

At the present time, the perfluorosulfonate ionomer membranes, such as Nafion membrane (Dupont), are mainly used on the DMFC. However, the commercial Nafion polymer membranes showed a serious methanol crossover problem [5,9], where methanol permeates from the anode to the cathode. The methanol permeation not only causes fuel loss but also forms a mixed potential at the cathode and reduces the electrochemical performance of the DMFC. Thus, the solid polymer membrane with lower methanol permeability is very important property for DMFC applications. For perfluorosulfonate membrane (Nafion), various ceramic fillers have been added into Nafion membranes to reduce the methanol crossover rate, such as TiO_2 [5,24], SiO_2 [25–32], montmorillonite (MMT) [33,34], zeolite [35,36], and Zr-phosphate [37] all of which have been widely studied. For non-perfluorosulfonate membranes, different composite polymer-based membranes for DMFCs have been extensively studied, for example, PVDF + Al_2O_3 [38], sulfonated styrene–(ethylene–butylene)-sulfonated styrene (SEBSS) + SiO_2 [39], sulfonated poly(ether ether ketone) + ZrO_2 [40], sPEEK + ZrPh [41], sPEEK + MCM-41 [42], etc.

Alkaline polymer electrolytes based on PVA [43–49] have been studied for application on Ni-MH, Zn-air, and DMFC cells. They reported the alkaline PVA-KOH polymer electrolyte exhibiting the ionic conductivity to be around

* Corresponding author. Tel.: +886 2 9089899; fax: +886 2 29041914.
E-mail address: ccyang@ccsun.mit.edu.tw (C.-C. Yang).

0378-7753/$ – see front matter © 2007 Elsevier B.V. All rights reserved.
doi:10.1016/j.jpowsour.2007.11.010

10^{-2}–10^{-1} S cm^{-1} at room temperature. Yang [49] also prepared the alkaline crosslinked PVA/TiO_2 nanocomposite polymer membranes applied on the DMFC. The maximum peak power density for alkaline DMFC was about 7.54 mW cm^{-2} at 60 °C and 1 atm.

Hydroxyapatite ($Ca_{10}(PO_4)_6(OH)_2$, HAP) has long been used as an implant material due to excellent biocompatibility, bioactivity and chemical stability. The addition of hydroxyapatite (HAP) ceramic filler into a polymer matrix not only facilitated a reduction of the glass transition temperature (T_g) and the crystallinity of the PVA polymer, but also increased the amorphous phases of the polymer matrix as well as its ionic conductivity. As we know, when the HAP filler, which is a stiffer material, is added to the PVA matrix, the swelling ratio of PVA/HAP composite polymer membrane is effectively reduced. As a result, the mechanical properties, dimension stability and swelling ratio of the polymer membrane are also improved.

Yu and Scott [50–52] recently studied the electrochemical performance of the alkaline DMFC with anion-exchange membranes. The DMFC performance with a maximum power density of about 10 mW cm^{-2} was obtained in a commercial quaternary-ammonium anion-exchange membrane (Morgane-ADP, Solvay SA, Belgium). In addition, Rhim et al. [53] and Lin et al. [54] prepared PVA/PWA polymer electrolyte membranes and applied them to the DMFC. Varcoe et al. [55–58] developed and characterized the quaternary-ammonium (as the counter ions bound to the polymer backbone) radiation grafted ETFC [55], PVDF and FEP [58] alkaline anion-exchange membrane (AAEM). They prepared the AAEM-MEAs that do not contain any metal-cation M^{n+} (i.e., K^+, Na^+) to avoid the carbonate precipitation problem and to improve long-term operation stability. This preparation proved to be a breakthrough for alkaline anion-exchange membranes on fuel cell applications. The peak power density of 130 mW cm^{-2} for the H_2/O_2 fuel cell with AAEM membrane was obtained, while the maximum power density of 8.5 mW cm^{-2} was obtained in a metal-cation-free methanol/O_2 fuel cell with 2–2.5 bar back pressure at 80 °C.

Those experimental results indicated that when different ceramic fillers were added into the solid polymer electrolyte (SPE), ionic conductivity, thermal and mechanical properties were improved. The increase of ionic conductivity of the composite polymer electrolyte can be explained by the fact that the HAP fillers in the polymer matrix created some defects or voids at the boundaries of between the ceramic particles and the polymer chain. In this composite polymer membrane there was a dispersion of the HAP ceramic fillers into the PVA matrix, which acted as a solid plasticizer capable of enhancing chemical, thermal and mechanical stabilities for the composite polymer membranes.

TGA was used to analyze the thermal stability properties of the PVA/HAP composite polymer membrane. The crystallinity and surface morphology of the PVA/HAP composite polymer membranes were examined by XRD and SEM, respectively. Micro-Raman spectroscopy was applied to study the chemical composition of the PVA/HAP polymer membranes. The ionic conductivity of alkaline PVA/HAP composite polymer electrolytes was measured by AC impedance spectroscopy. The characteristic properties of the crosslinked PVA/HAP polymer membranes with different weight percentages of HAP fillers (2.5–10 wt.%) will be examined and discussed in detail.

In this work, the alkaline DMFC, composed of the air cathode electrode loaded with MnO_2/BP2000 carbon inks, the PtRu anode electrode (4.00 mg cm^{-2}) and the PVA/HAP composite polymer membranes, was assembled and examined. The PVA/HAP composite polymer membranes were first prepared through direct blending of PVA with HAP fillers under ultrasonic condition. The composite polymer membranes obtained from this process were further crosslinked by adding 5 wt.% glutaraldehyde (GA) solution. For anodic methanol electrooxidation reaction, cathodic oxygen reduction reaction (ORR) and the overall reaction of the DMFC in alkaline media can be described as follows:

- Anodic reaction:

$$CH_3OH + 6OH^- \rightarrow CO_2 + 5H_2O + 6e^-, \quad E_a^0 = -0.810\,\text{V (vs. SHE)}, \tag{1}$$

- Cathodic reaction:

$$1.5O_2 + 3H_2O + 6e^- \rightarrow 6OH^-, \quad E_c^0 = 0.402\,\text{V (vs. SHE)}, \tag{2}$$

- Overall reaction:

$$CH_3OH + 1.5O_2 \rightarrow CO_2 + 2H_2O, \quad E_{cell}^0 = 1.21\,\text{V}, \tag{3}$$

Additionally, the electrochemical characteristics of the DMFCs with alkaline PVA/HAP composite polymer membranes were investigated by the linear polarization, galvonostatic and potentiostatic methods; especially, for the peak power density of the DMFC.

2. Experimental

2.1. Preparation of the PVA/HAP composite polymer membranes

PVA (Aldrich), HAP ceramic fillers (Aldrich), and KOH (Merck) were used as-received without further purification. Degree of polymerization and saponification of PVA were 1700 and 98–99%, respectively. The PVA/HAP composite polymer membranes were prepared by a solution casting method. The appropriate weight ratios of PVA:HAP = 1:2.5–15 wt.% were dissolved in distilled water by stirring. The PVA/HAP composite polymer membranes were further crosslinked by adding a 5 wt.% glutaraldehyde solution (GA, 25% content in distilled water, Merck) and 1.0 vol.% HCl (HCl used as a catalyst) in the bath. The above resulting solution was stirred continuously until the solution mixture reached a homogeneous viscous appearance at 90 °C for 2 h. The blending time of PVA polymer and HAP fillers was well controlled. The resulting viscous solution was poured out into a Petri dish. The thickness of the wet composite polymer membranes was between 0.20 and 0.40 mm. The Petri

dish with viscous PVA/HAP composite polymer sample was weighed again and then the excess water solvent was allowed to evaporate slowly at 25 °C at a relative humidity of 30%. The Petri dish with the PVA/HAP composite polymer membrane was weighed again after the composite polymer membrane was dried. The composition of the PVA/HAP composite polymer membrane was determined by mass balance. The thickness of the composite polymer membranes was controlled within the range of 0.10–0.30 mm. The preparation methods of the PVA-based polymer electrolyte membranes by the solution casting method have been reported in detail elsewhere [43–49].

2.2. Ionic conductivity measurements, liquid uptake and swelling ratio

Conductivity measurements were made for alkaline PVA/HAP composite polymer membranes by an AC impedance method. The PVA/HAP composite samples were immersed in 8 M KOH solutions for at least 24 h before testing. The alkaline PVA/HAP composite polymer membranes were placed between SS304 stainless steel, ion-blocking electrodes, with a surface area of 1.32 cm^2, in a spring-loaded glass holder. A thermocouple was kept close to the composite polymer membrane for temperature measurement. Each sample was equilibrated at the experimental temperature for at least 30 min before measurement. AC impedance measurements were carried out using Autolab PGSTAT-30 equipment (Eco Chemie B.V., Netherlands). An AC frequency range of 300 kHz–10 Hz at an excitation signal of 5 mV was recorded. The impedance of the composite polymer membrane was recorded at a temperature range of 30–70 °C. Experimental temperatures were maintained within ±0.5 °C by a convection oven. All alkaline PVA/HAP composite polymer membranes were measured at least three times.

The pre-weighted and dried PVA/HAP composite polymer membrane (W_0) was immersed in DI water, 99 wt.%CH_3OH, 4 M KOH aqueous solutions, respectively, and maintained for 24 h at 25 °C until equilibrium was established. The composite polymer membrane was taken out from the immersion bath and the excess surface water was carefully removed. The weight of the wet composite polymer membrane (W_1) was then determined. The percentages of liquid absorption and swelling ratio were calculated from the following equation:

$$\text{Absorption}\,(\%) = \frac{W_1 - W_0}{W_1} \times 100 \quad (4)$$

$$\text{Swelling ratio}\,(\%) = \frac{W_1 - W_0}{W_0} \times 100 \quad (5)$$

2.3. Thermal property, crystallinity and morphology analyses

TGA thermal analysis was carried out using a PerkinElmer Pyris 7 TGA system. The measurements were carried out by heating from 25 to 500 °C, under N_2 atmosphere at a heating rate of 10 °C min^{-1} with about 10 mg samples. The crystal structures of all PVA/HAP composite polymer membranes were examined using a Philips X'Pert X-ray diffractometer (XRD) with Cu Kα radiation of wavelength λ = 1.54056 Å for 2θ angles between 10 and 90°. The surface morphology and microstructure of the PVA/HAP composite polymer membrane were examined by a Hitachi S-2600H scanning electron microscope (SEM).

2.4. Micro-Raman spectroscopy analyses

Raman spectrum is a unique tool used to characterize the PVA/HAP composite polymer membrane. The micro-Raman spectroscopy analysis was carried out by a Renishaw confocal microscopy Raman spectroscopy system with a microscope equipped with 10×, 20×, and 50× objectives, and a charge-coupled device (CCD) detector. Raman excitation source was provided by a 514 nm laser beam, which had the beam power 25 mW and was focused on the sample with a spot size of about 1 μm in diameter.

2.5. Preparation of the anode and cathode electrodes

The preparation of the catalyst slurry ink for the anode electrode was prepared by mixing 70 wt.% PtRu black inks (Alfa, HiSPEC 6000, PtRu black with Pt:Ru = 1:1 molar ratio), 30 wt.% PTFE binder solution (Dupont, 30 wt.% base solution), and a suitable amount of distilled water and alcohol. The resulting PtRu black mixtures were ultrasonicated for 2 h. The PtRu black inks were loaded onto the carbon paper (SGL GDL 10 BC, Germany) by a paint-brush method to obtain a loading of PtRu black of 4.0 mg cm^{-2}. The as-prepared PtRu anode electrode was dried in a vacuum oven at 100 °C for 2 h.

The carbon slurry for the gas diffusion layer of the air cathode was prepared with a mixture of 70 wt.% Shawinigan acetylene black (AB50) with specific surface area of 80 m^2 g^{-1} and 30 wt.% PTFE (Teflon-30J suspension) as a wet-proofing agent and binder. The carbon slurry was coated on the Ni-foam as a current collector and then pressed at 100 kg_f cm^{-2}. The gas diffusion layer was then sintered at temperature of 375 °C for 30 min. The catalyst layer of the air electrode was then prepared by spraying a mixture of a 15 wt.% of PTFE solution binder and 85 wt.% of mixed powders consisting of γ-MnO_2 (electrolytic manganese oxide, EMD) catalyst supported on BP2000 carbon black. The Ni-foam current collector was cut at 1 × 1 cm^2. The preparation methods of the air cathode electrodes have been reported in detail elsewhere [59,60].

2.6. Electrochemical measurements

The PVA/HAP composite polymer membranes were placed between the sheets of the anode electrode and the cathode electrode, and then hot-pressed at 60 °C with a pressure of 100 kg_f cm^{-2} for 5 min to obtain a membrane electrode assembly (MEA). The electrode area of the MEA was about 1 cm^2.

The electrochemical measurements were carried out in a two-electrode system. The *E–t* or *i–t* curves of the DMFCs with alkaline PVA/HAP composite polymer membranes were recorded at various current densities of 20–40 mA cm^{-2} and at different cell potentials (0.20–0.40 V). All electrochemical

measurements were performed on an Autolab PGSTAT-30 electrochemical system with GPES 4.8 package software (Eco Chemie, The Netherland). The electrochemical performances of the DMFC employing the PVA/HAP composite polymer membrane with the cathode electrode open to atmospheric air were studied in 8 M KOH + 2 M CH_3OH solutions at ambient temperature and pressure. The construction of alkaline DMFC for testing has been described in detail elsewhere [49].

3. Results and discussion

3.1. TGA thermal analysis

Fig. 1(a) shows TGA and differential gravimetric analysis (DTG) thermographs of the PVA polymer membrane without GA (un-crosslinked sample) and the PVA polymer membrane with 5 wt.% GA (crosslinked sample), respectively. The TGA and DTG curves of the un-crosslinked PVA polymer film reveal two main weight loss regions, which appear as two peaks in the DTG curves. The first peak transition region at around 282 °C is due to the degradation of PVA polymer membrane; the total weight loss corresponds to this stage at about 77 wt.%. The peak of the second stage at 424 °C is due to the cleavage C–C backbone of PVA polymer membrane, the so-called carbonation; the total weight loss was 91 wt.% at 600 °C.

Table 1
The results of weight loss (%) of the PVA/HAP composite polymer membranes at various temperatures

Types	Temperature (°C)			
	100	250	350	600
HAP powders	0.68	6.81	2.79	3.49
PVA film	0.63	8.00	73.10	92.24
PVA/2.5 wt.%HAP	3.75	12.13	35.98	90.67
PVA/5 wt.%HAP	2.93	7.26	27.96	91.90
PVA/10 wt.%HAP	2.58	6.81	27.39	87.06

TGA and DTG curves of the crosslinked PVA polymer membranes with GA also display two main weight losses, which also appear as two peaks in the DTG curves. The first peak transition at around 197 °C may be due to the degradation of GA; the total weight loss corresponds to this stage at about 15 wt.%. The third peak at 450 °C is caused on account of the breaking of the main chain of the PVA polymer; so that there was a total weight loss of 91 wt.% at 600 °C. By comparison, the second main weight loss is obviously less intense, as compared with the un-crosslinked PVA polymer film. Table 1 lists the percentages of weight loss for PVA and crosslinked PVA polymer membranes at different stage temperatures. Thermal stability of the PVA membrane is improved by the crosslinked treatment.

Fig. 1(b) demonstrates shows TGA and DTG thermographs of HAP powders and the PVA/HAP composite polymer membranes with various HAP compositions. Those curves of the PVA/HAP polymer film reveal two main weight loss regions, which also appear as two peaks in the DTG curves. The first transition region at around 350–380 °C ($T_{max,1}$ = 363 °C) is

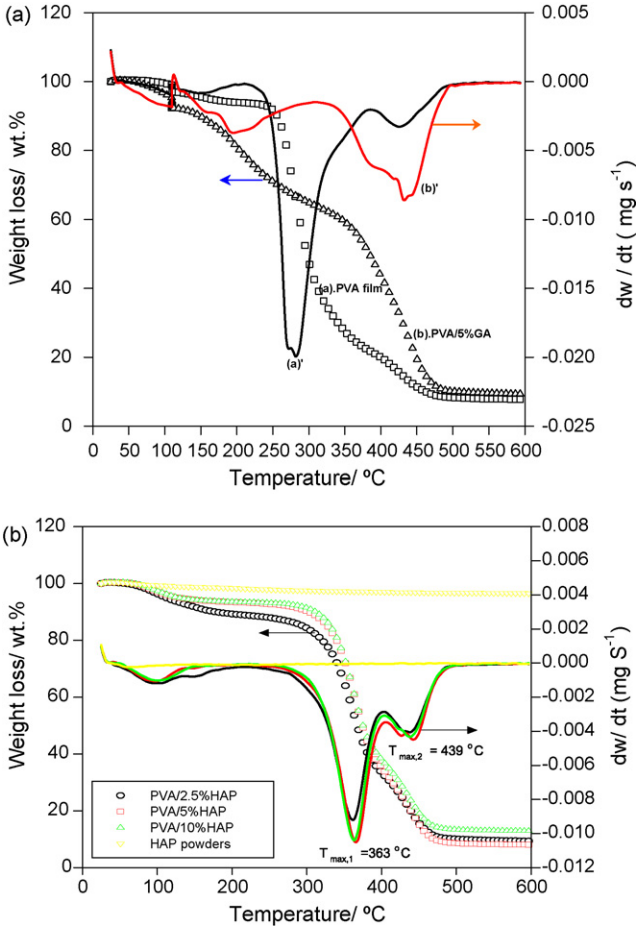

Fig. 1. TGA thermographs of the PVA, PVA/GA, and crosslinked PVA/HAP composite polymer membranes with different compositions of HAP fillers.

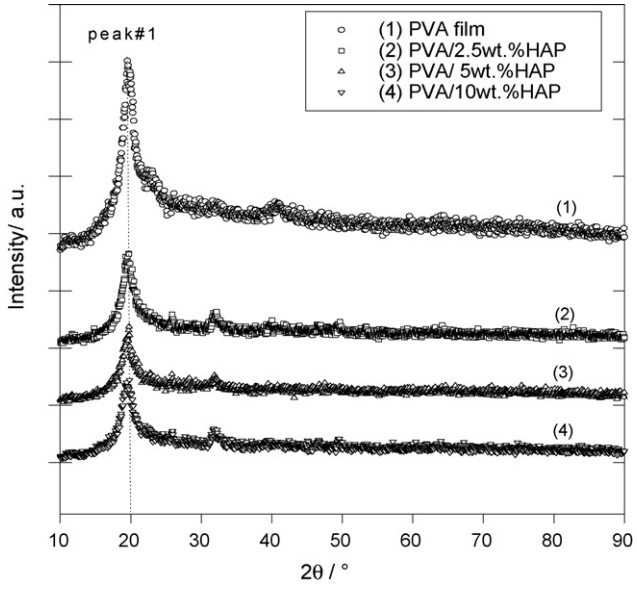

Fig. 2. XRD patterns for the PVA/HAP composite polymer membranes with different HAP compositions.

due to the degradation of PVA polymer membrane; the total weight loss corresponding to this stage was about 38–46 wt.%. The second peak at 439 °C ($T_{max,2}$ = 439 °C) leads to the cleavage backbone of PVA polymer membrane and the total weight loss was about 90 wt.% at 600 °C, as displayed in Table 1.

Overall, the degradation peaks of the crosslinked PVA/HAP composite polymer samples are less intense and shift towards higher temperatures. It can be concluded that the thermal stability is improved due to the effect of HAP ceramic fillers and the chemical crosslinking treatment.

3.2. Crystallinity, surface morphology and micro-Raman analysis

The X-ray diffraction measurement was performed to examine the crystallinity of the PVA/HAP composite polymer membranes. Fig. 2 illustrates the diffraction pattern of the PVA/HAP composite polymer membranes that were prepared by a blending process with different HAP compositions. The PVA polymer is well known to exhibit a semi-crystalline structure with a large peak at a 2θ angle of 19–20° and a small peak of 39–40° [43–49]. A large peak at 2θ = 19–20° for

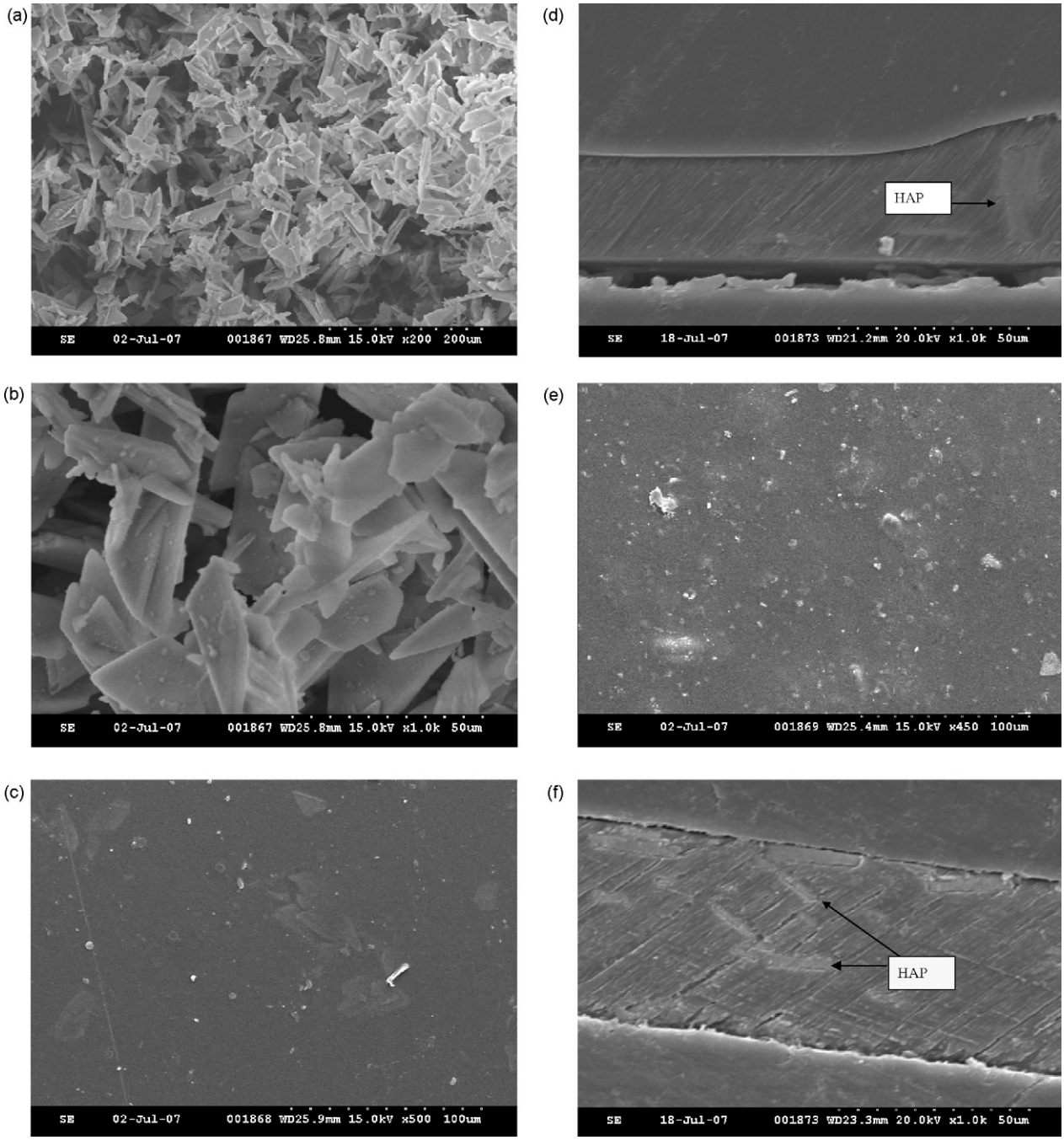

Fig. 3. SEM photographs: (a) top view of HAP fillers at 200×; (b) top view of HAP fillers at 1000×; (c) top view for PVA/5 wt.%HAP SPE; (d) cross-sectional view for PVA/5 wt.%HAP; (e) top view for PVA/10 wt.%HAP SPE; (f) cross-sectional view for PVA/10 wt.%HAP SPE; (g) cross-sectional view for PVA/15 wt.% SPE.

(g)

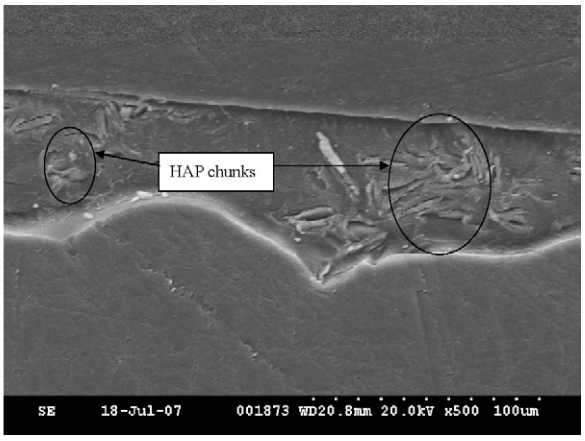

Fig. 3. (*Continued*).

the PVA/2.5–10 wt.%HAP composite polymer membranes was clearly seen in Fig. 2. But, the peak intensity of XRD for the PVA/HAP composite polymer films was obviously reduced when the amount of added HAP fillers increased. Under such circumstances, it was clear that the amorphous domain in the PVA/HAP composite polymer membranes was greatly augmented (i.e., the degree of crystallinity decreased).

Table 2 shows the values of relative crystallinity (%) for the PVA/HAP composite polymer membranes with different compositions of HAP fillers. The relative crystallinity values of the PVA/HAP composite polymer membrane decreased from 100 to 30.53%. Note that the degree of amorphous domain increases with an increase in the contents of HAP fillers. There is a significant motion of the polymer chain in the amorphous phase or some defects existing at an interface between the polymer chains and the crystal HAP fillers at the same time as there is non-conductivity the crystalline phase. Therefore, the characteristic of the PVA/HAP composite polymer membranes shows good ionic conductivity transport property (data shown in Section 3.3). This is due to the more amorphous phase and flexible of local PVA chain segmental motion in the PVA/HAP composite polymer membranes.

SEM photographs for the as-received HAP powders at different magnifications (200× and 1000×) are shown in Fig. 3(a) and (b), respectively. As SEM photographs indicated, the HAP powders have a flake-like structure with different sizes. The top and cross-sectional views of SEM photographs for the PVA/5 wt.%HAP composite polymer membranes can be found in Fig. 3(c) and (d), respectively. Moreover, the top and cross-sectional view of SEM photographs for the PVA/10 wt.%HAP composite polymer membranes are also shown in Fig. 3(e) and (f), respectively. Furthermore, these HAP fillers are found to disperse well into the PVA polymer matrix. The dimension for the HAP fillers embedded in PVA matrix is about 2 μm × 20 μm with flake-like shape, as shown in Fig. 3(f). Fig. 3(g) particularly shows the cross-sectional view of SEM photograph for the PVA/15 wt.%HAP composite polymer membrane at 500×. Where large HAP aggregates or chunks are clearly formed and located at different positions of the PVA matrix, the HAP fillers were not dispersed well.

Table 2
The percentages of relative crystallinity of PVA/HAP composite polymer membranes

Type	Position of peak#1 (°)	Intensity of peak#1	Relative crystallinity (%)[a]
PVA film	19.77	704	100.0
PVA + 5%GA film	19.77	316	44.88
PVA/2.5 wt.%HAP + 5 wt.%GA	19.77	268	38.07
PVA/5 wt.%HAP + 5 wt.%GA	19.77	228	32.38
PVA/10 wt.%HAP + 5 wt.%GA	19.77	215	30.53

[a] Based on peak#1 of XRD data.

As a whole, the compatibility of the PVA polymer and HAP fillers is uniform and homogenous when the content of HAP ceramic fillers is less than 10 wt.%. As we know, the higher content of HAP fillers (as a methanol permeation barrier) in the PVA matrix may assist in reducing the methanol crossover through the composite polymer membrane.

Fig. 4 shows the micro-Raman spectra for HAP powders and PVA/HAP composite polymer membranes with different compositions of HAP fillers. It can be seen clearly from the micro-Raman spectra that the strong characteristic scattering peak of HAP fillers at 958 cm^{-1} is associated with the HAP filler; this is due to the P–O band stretching. By contrast, the strong peak for the PVA polymer at 1437 cm^{-1} is due to the C–H bending and O–H bending. Moreover, the two weak vibrational peaks for the PVA polymer at 912 and 851 cm^{-1} are due to the C–C stretching. Finally, there are several weak scattering peaks at 1145 and 1088 cm^{-1}; which are caused by the C–C stretching and C–O stretching. Interestingly, the peak intensity of the 1147 cm^{-1} band is an indicator of the degree of crystallinity of the PVA polymer [61]. The peak intensity of the 1147 cm^{-1} band decreased when the amount of HAP fillers added was increased. It can be clearly seen that the intensities of the 1147 cm^{-1} characteristic vibrational peak of all PVA/HAP composite polymer membranes are greatly decreased and the result indicates the amorphous phases in the PVA/HAP composite polymer membrane were augmented. The higher the percentage of amorphous domains of the PVA/HAP, the higher the value of ionic conductivity which can be obtained.

3.3. Ionic conductivities measurement, liquid absorption, and swelling ratio

The typical AC impedance spectra (the so-called Nyquist plot) of alkaline PVA/HAP composite polymer membranes by a direct blending of PVA polymer with the HAP fillers (5 wt.%) at different temperatures are shown in Fig. 5. The AC spectra are typically non-vertical spikes for stainless steel (SS) blocking electrodes, i.e., the SS|PVA/HAP SPE|SS cell. Analysis of the spectra yields information about the properties of the PVA/HAP polymer electrolyte, such as bulk resistance, R_b. Taking into account the thickness of the composite electrolyte films, the R_b value was converted into the ionic conductivity value, σ, according to the equation: $\sigma = L/R_b \times A$, where L is the thickness (cm) of the PVA/HAP polymer membrane, A is the area of the blocking electrode (cm^2), and R_b is the bulk

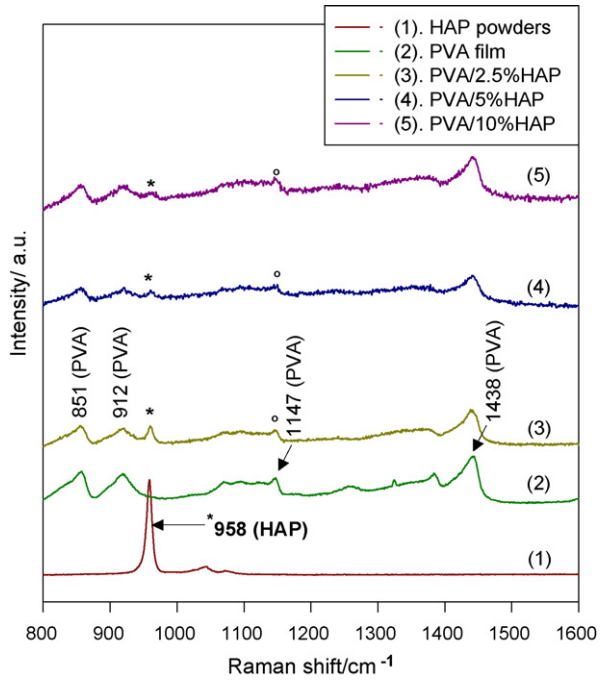

Fig. 4. Micro-Raman spectra for the PVA/HAP composite polymer membranes with different amounts of HAP fillers.

resistance (Ω) of the alkaline PVA/HAP composite polymer electrolyte.

Typically, the R_b values for the blend PVA/HAP composite polymer membranes are of the order of 1–2 Ω and are dependent on the contents of HAP fillers and KOH in the film. Note that, the composite polymer membrane was immersed in 8 M KOH solution for 24 h before measurement. Table 3 shows the ionic conductivities of the alkaline PVA/HAP (2.5 wt.%) composite polymer membrane at different temperatures. As a result, the ionic conductivity value is 0.0182 S cm^{-1} at 30 °C.

Table 3
The ionic conductivity values of PVA/HAP composite polymer membranes with different compositions of HAP fillers

T (°C)	HAP contents (σ, S cm^{-1})		
	2.5 wt.%HAP	5 wt.%HAP	10 wt.%HAP
30	0.0182	0.0251	0.0442
40	0.0212	0.0272	0.0465
50	0.0263	0.0295	0.0483
60	0.0314	0.0315	0.0514
70	0.0378	0.0335	0.0542

The ionic conductivity values of alkaline PVA/HAP composite polymer membrane with 5 and 10 wt.%HAP fillers are 0.0251 and 0.0442 S cm^{-1} at 30 °C, respectively. The data shows the highest ionic conductivity of alkaline PVA/HAP composite polymer membrane is 0.0442 S cm^{-1} with 10 wt.%HAP fillers at an ambient temperature. These results can be determined as the ionic conductivity of the PVA/HAP composite polymer membranes increases when the content of added HAP fillers increases.

In general, when the HAP fillers are added into the PVA polymer membrane, more accessible amorphous phases (or more defects) appear and enhance its ionic mobility. It was observed that the ionic conductivity is of the order in 10^{-2} S cm^{-1} at ambient temperature. The temperature dependence of the ionic conductivity obeys the Arrhenius type: $\sigma = \sigma_0 \exp(-E_a/RT)$, where σ_0 is a pre-exponential factor, E_a is the activation energy, and T is the temperature in K. The $\log_{10}(\sigma)$ vs. $1/T$ plots, as shown in Fig. 6, obtains the activation energy (E_a) of the PVA/HAP composite SPE, which is highly dependent on the contents of HAP fillers and KOH electrolyte. The E_a value for alkaline PVA/5 wt.%HAP composite polymer membrane is 4.37 kJ mol^{-1}; the E_a value for the crosslinked SPEs normally appears as over 20 kJ mol^{-1}. It is well known that E_a is related

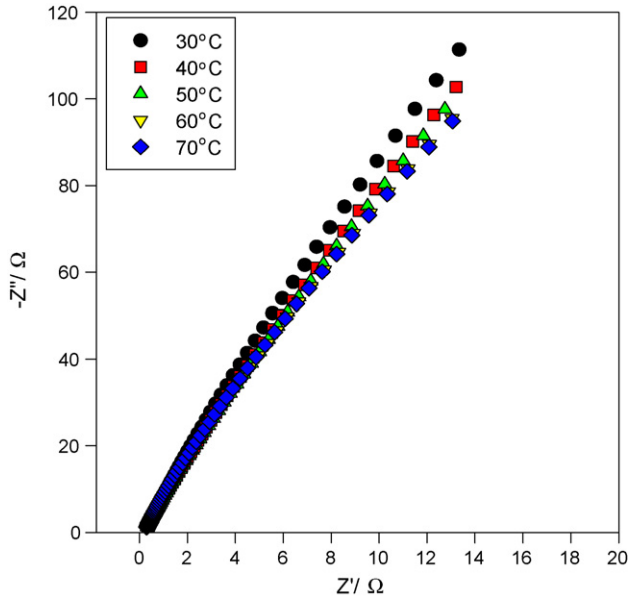

Fig. 5. Nyquist plot for alkaline PVA/5 wt.%HAP composite polymer membrane.

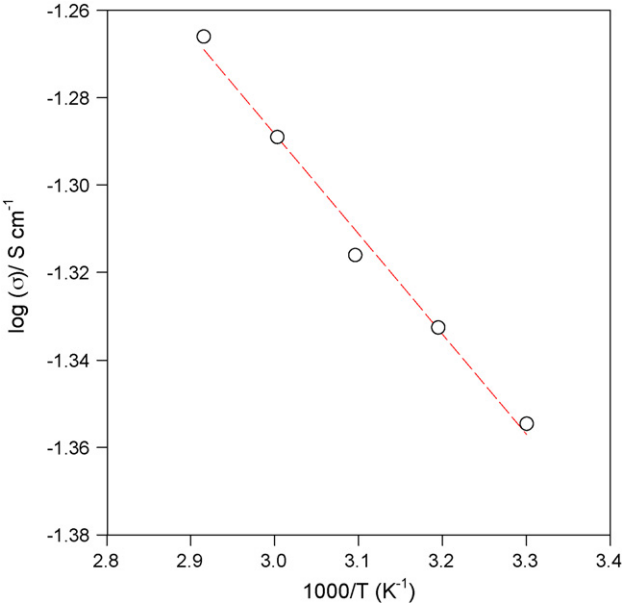

Fig. 6. Arrhenius plot of alkaline PVA/5 wt.%HAP composite polymer membrane.

Table 4
The results of liquid absorption (%) of the PVA/HAP composite polymer membranes at 25 °C

Absorption	Types		
	PVA/2.5 wt.%HAP	PVA/5 wt.%HAP	PVA/10 wt.%HAP
DI water	60.5%	55.3%	45.0%
99 wt.%CH_3OH	16.4%	15.0%	14.8%
4 M KOH	47.6%	38.3%	36.6%

to its ionic mobility (μ_i), because $\sigma = \sum F|Z_i|C_i\mu_i$, where σ is the ionic conductivity, F is Faraday constant, Z_i is the charge number, C_i is the carrier concentration, and μ_i is the mobility [62]. Consequently, it can be considered that the increase of ionic conductivity accomplished by adding HAP fillers is mainly related to its ionic mobility (μ_i), which indicates the more segmental motion in the amorphous phase of the PVA matrix, resulting in the higher ionic mobility and ionic conductivity.

Besides, the dimension stability of the PVA/HAP composite polymer membranes is also crucial for practical applications. The results of liquid absorption (%) values of PVA/HAP composite polymer membranes in DI water, 99 wt.%CH_3OH, 4 M KOH solutions are shown in Table 4. The absorption percentage of DI water slightly decreases from 60.5 to 45.0 wt.% when the amount of added HAP fillers increases from 2.5 to 10 wt.%. Furthermore, the absorption percentage of CH_3OH solution remains steadily around 14–16 wt.% while the absorption percentage of 4 M KOH solution decreases from 47.6 to 36.6 wt.% as the amount of added HAP fillers increases.

By contrast, the results of swelling ratio (%) for the PVA/HAP composite polymer membranes in DI water, 99 wt.%CH_3OH, 4 M KOH solutions are listed in Table 5. The data demonstrate that the swelling ratio value of the PVA/HAP composite polymer membranes in DI water significantly decreases from 122.4 to 88 wt.% as the amount of HAP fillers added increases from 2.5 to 10 wt.%. The swelling ratio in 99 wt.%CH_3OH is around 17–19 wt.%; furthermore, the swelling ratio in 4 M KOH solution greatly decreases from 91 to 55 wt.%. When the HAP filler as a stiffer material is added into the PVA matrix, the swelling ratio of PVA polymer membranes can be effectively reduced. Obviously, the thermal properties, ionic conductivity and dimension stability are improved.

Table 5
The results of swelling ratio (%) of the PVA/HAP composite polymer membranes at 25 °C

Swelling	Types		
	PVA/2.5 wt.%HAP	PVA/5 wt.%HAP	PVA/10 wt.%HAP
DI water	122.4%	112.9%	88.4%
99 wt.%CH_3OH	19.7%	17.6%	17.4%
4 M KOH	90.7%	67.5%	54.7%

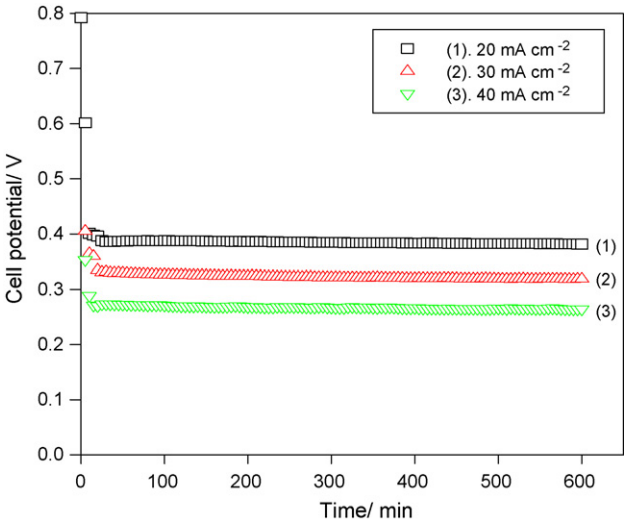

Fig. 7. The *E–t* curves for the DMFC employing the PVA/10 wt.%HAP composite polymer membrane in 8 M KOH + 2 M CH_3OH solution at 25 °C and 1 atm.

3.4. Electrochemical characterization of alkaline DMFC

Fig. 7 shows the *E–t* curves of alkaline DMFC consisting of the anode electrode with a loading of PtRu black of 4.0 mg cm^{-2}, the cathode electrode with MnO_2/BP2000 carbon inks of 3.63 mg cm^{-2} and the PVA/10 wt.%HAP composite polymer membrane in 8 M KOH + 2 M CH_3OH solutions at 20, 30 and 40 mA cm^{-2} at 25 °C, respectively. In spite of a tendency to fall at the beginning of the test, the cell potential is stable and remains constant for 10 h test; it shows good electrochemical stability of alkaline DMFC.

Fig. 8 shows the *i–t* curves of an air-breathing DMFC employing the PVA/10 wt.%HAP composite polymer membrane in 8 M KOH + 2 M CH_3OH solution at 0.40, 0.30 and 0.20 V at 25 °C,

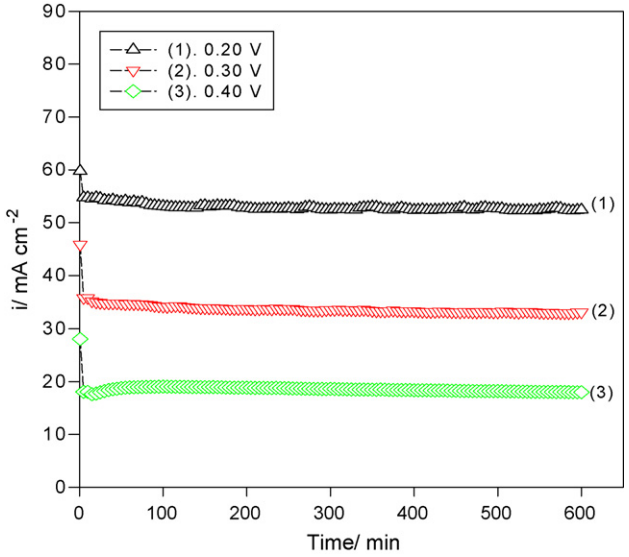

Fig. 8. The *i–t* curves for the DMFC employing the PVA/10 wt.%HAP composite polymer membrane in 8 M KOH + 2 M CH_3OH solution at 25 °C and 1 atm.

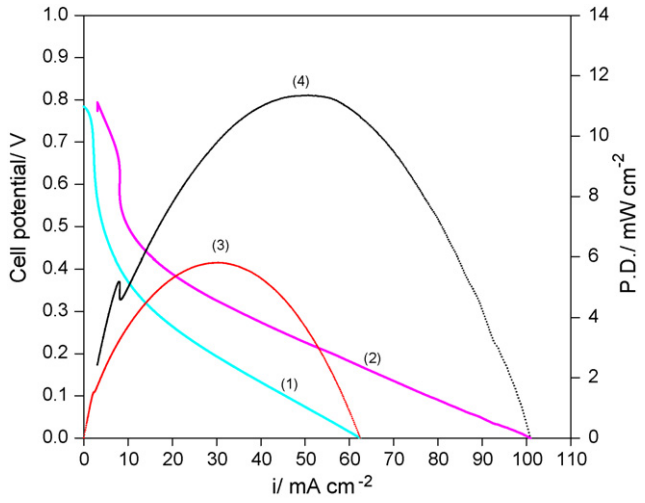

Fig. 9. The IV and PD curves for the DMFC employing the PVA/10%HAP composite polymer membrane in 8 M KOH + 2 CH_3OH solution at 25 °C and 1 atm; (1) IV curve for E-TEK anode; (2) IV curve for Ti-based anode; (3) PD curve for E-TEK anode; (4) PD curve for Ti-based anode.

respectively. The average current densities of the DMFC are 18.59, 33.84, and 52.96 mA cm^{-2}, respectively. Although the discharge current densities dropped at the beginning of the test, it was soon stabilized and remained constant for 10 h. The result revealed an improved electrochemical performance of the DMFC. According to the result of Fig. 8, the power density of the air-breathing DMFC in 8 M KOH + 2 M CH_3OH solution at 0.20 V is 10.59 mW cm^{-2} (0.20 V × 52.96 = 10.59 mW cm^{-2}) at 25 °C.

Fig. 9 illustrates the potential–current density and the power density–current density curves of an air-breathing DMFC in 8 M KOH + 2 M CH_3OH solution at 25 °C. The maximum power density of 11.48 mW cm^{-2} of the air-breathing DMFC employing the Ti-based anode with 4 mg cm^{-2} PtRu black was clearly achieved at $E_{p,max}$ = 0.22 V with a peak current density ($i_{p,max}$) of 52.20 mA cm^{-2}. On the other hand, the maximum power density of the air-breathing DMFC using a ELAT anode with 4 mg cm^{-2} PtRu/C was only about 5.81 mW cm^{-2} at $E_{p,max}$ = 0.190 V with a peak current density of 30.58 mA cm^{-2} at 25 °C.

Scrosati and coworkers [7] prepared the PVA/SiO_2 composite polymer membrane for a lab-type acidic DMFC using a 2 M H_2SO_4 + 2 M CH_3OH solution, with the DMFC being at a maximum peak power density of about 2.0 mW cm^{-2} at the ambient temperature and pressure. Furthermore, it was found from their results that the stability of MEA with Nafion polymer membrane seems unstable for their lab-type DMFC. By contrast, the electrochemical performance of alkaline DMFC using the crosslinked PVA/HAP composite membrane (PD = 11.48 mW cm^{-2}) is better than that of acidic DMFC cell with the crosslinked PVA/SiO_2 composite membrane (PD = 2.00 mW cm^{-2}) at ambient conditions. The alkaline DMFC system apparently exhibits some advantages over than that of the acidic DMFC system. This alkaline DMFC consists of the air electrode using a non-precious metal catalyst (i.e., with MnO_2/BP2000 catalyst inks instead of with Pt/C inks) and a low-cost PVA/HAP composite polymer membrane (i.e., a cheap non-perfluorosulfonated polymer membrane instead of Nafion) is particularly worthy of notice.

4. Conclusions

The composite polymer membrane based on PVA/HAP was prepared by a solution casting method. Alkaline air-breathing direct methanol fuel cell (DMFC) utilizing the PVA/HAP composite polymer membrane was assembled and systematically studied. The air-breathing DMFC was comprised of the air cathode electrode with MnO_2/BP2000 catalyst inks, the PtRu Ti-anode electrode and the PVA/HAP composite polymer membrane. The results demonstrated that alkaline air-breathing DMFC with the PVA/HAP composite polymer membrane shows good electrochemical performances at ambient temperatures and pressure. The maximum peak power density of the DMFC is 11.48 mW cm^{-2} at ambient air and temperature. From the application point of view, these composite polymer membranes show a high potential for the DMFC applications.

Acknowledgement

Financial support from the National Science Council, Taiwan (project no: NSC-95-2221-E131-032) is gratefully acknowledged.

References

[1] W.H. Lizcano-Valbuena, V.A. Paganin, E.R. Gonzalez, Electrochim. Acta 47 (2002) 3715.
[2] N. Nakagawa, Y. Xiu, J. Power Sources 118 (2003) 248.
[3] G.G. Park, T.H. Yang, Y.G. Yoon, W.Y. Lee, C.S. Kim, Int. J. Hydrogen Energy 28 (2003) 645.
[4] H. Fukunaga, T. Ishida, N. Teranishi, C. Arai, K. Yamada, Electrochim. Acta 49 (2004) 2123.
[5] V. Baglio, A.S. Arico, A.D. Blasi, V. Antonucci, P.L. Antonucci, S. Licoccia, E. Traversa, F.S. Fiory, Electrochim. Acta 50 (2005) 1241.
[6] T.C. Deivaraj, J.Y. Lee, J. Power Sources 142 (2005) 43.
[7] S. Panero, P. Fiorenza, M.A. Navarra, J. Romanowska, B. Scrosati, J. Electrochem. Soc. 152 (12) (2005) A2400.
[8] K. Furukawa, K. Okajima, M. Sudoh, J. Power Sources 139 (2005) 9.
[9] J.H. Choi, Y.M. Kim, J.S. Lee, K.Y. Cho, H.Y. Jung, J.K. Park, I.S. Park, Y.E. Sung, Solid State Ionics 176 (2005) 3031.
[10] V.S. Silva, S. Weisshaar, R. Reissner, B. Ruffmann, S. Vetter, A. Mendes, L.M. Madeirs, S. Nunes, J. Power Sources 145 (2005) 485.
[11] B.E. Hayden, D.V. Malevich, D. Pletcher, Electrochem. Commun. 3 (2001) 395.
[12] E. Antolini, Mater. Chem. Phys. 78 (2003) 563.
[13] G.Q. Lu, C.Y. Wang, J. Power Sources 144 (2005) 141.
[14] C.Y. Chen, P. Yang, J. Power Sources 123 (2003) 37.
[15] T. Shimizu, T. Momma, M. Mohamedi, T. Osaka, S. Sarangapani, J. Power Sources 137 (2004) 277.
[16] K. Kordesch, V. Hacker, U. Bachhiesl, J. Power Sources 96 (2001) 200.
[17] J.G. Liu, T.S. Zhao, R. Chen, C.W. Wong, Electrochem. Commun. 7 (2005) 288.
[18] B.K. Kho, I.H. Oh, S.A. Hong, H.Y. Ha, Electrochim. Acta 50 (2004) 781.
[19] V.S. Silva, B. Ruffmann, S. Vetter, M. Boaventura, A.M. Mendes, L.M. Madeira, S.P. Nunes, Electrochim. Acta 51 (2006) 3699.
[20] J.G. Liu, T.S. Zhao, Z.X. Liang, R. Chen, J. Power Sources 153 (2006) 61.
[21] Z.X. Liang, T.S. Zhao, J. Prabhuram, J. Membr. Sci. 283 (2006) 219.
[22] J. Prabhuram, T.S. Zhao, Z.X. Liang, H. Yang, C.W. Wong, J. Electrochem. Soc. 152 (7) (2005) A1390.

[23] Z.X. Liang, T.S. Zhao, J. Phys. Chem. C 111 (22) (2007) 8128.
[24] Z. Liu, B. Guo, J. Huang, L. Hong, M. Han, L.M. Gan, J. Power Sources 157 (2006) 207.
[25] P. Staiti, A.S. Arico, V. Baglio, F. Lufrano, E. Passalacqua, V. Antonucci, Solid State Ionics 145 (2001) 101.
[26] P.L. Antonucci, A.S. Arico, P. Creti, E. Ramunni, V. Antonucci, Solid State Ionics 125 (1999) 431.
[27] A.S. Arico, V. Baglio, A.D. Blasi, E. Modica, P.L. Antonucci, V. Antonucci, J. Power Sources 128 (2004) 113.
[28] V. Baglio, A.S. Arico, V. Antonucci, I. Nicotera, C. Oliviero, L. Coppola, P.L. Antonucci, J. Power Sources 163 (2006) 52.
[29] A.S. Arico, V. Baglio, A.D. Blasi, V. Antonucci, Electrochem. Commun. 5 (2003) 862.
[30] A.S. Arico, V. Baglio, V. Antonucci, I. Nicotera, C. Oliviero, L. Coppola, P.L. Antonucci, J. Membr. Sci. 270 (2006) 221.
[31] Y.J. Kim, W.C. Choi, S.I. Woo, W.H. Hong, J. Membr. Sci. 238 (2004) 213.
[32] A.S. Arico, V. Baglio, A.D. Blasi, P. Creti, P.L. Antonucci, V. Antonucci, Solid State Ionics 161 (2003) 251.
[33] Y.F. Lin, C.Y. Yen, C.H. Hung, Y.H. Hsiao, C.C.M. Ma, J. Power Sources 168 (2007) 162.
[34] F. Mura, R.F. Silva, A. Pozio, Electrochim. Acta 52 (2007) 5824.
[35] E.N. Gribov, E.V. Parkhomchuk, I.M. Krivobokov, J.A. Darr, A.G. Okunev, J. Membr. Sci. 297 (2007) 1.
[36] V. Baglio, A.D. Blasi, A.S. Arico, V. Antonucci, P.L. Antonuccci, F. Nannetti, V. Tricoli, Electrochim. Acta 50 (2005) 5181.
[37] F. Bauer, M. Willert-Porada, J. Membr. Sci. 233 (2004) 141.
[38] J. Shen, J. Xi, W. Zhu, L. Chen, X. Qiu, J. Power Sources 159 (2006) 894.
[39] D.H. Jung, Y.B. Myoung, S.Y. Cho, D.R. Shin, D.H. Peck, Int. J. Hydrogen Energy 26 (2001) 1263.
[40] V.S. Silva, B. Ruffmann, H. Silva, Y.A. Gallego, A. Mendes, L.M. Madeira, S.P. Nunes, J. Power Sources 140 (2005) 34.
[41] V.S. Silva, B. Ruffmann, S. Vetter, A. Mendes, L.M. Madeira, S.P. Nunes, Catal. Today 104 (2005) 205.
[42] C.S. Karthikeyan, S.P. Nunes, L.A.S.A. Prado, M.L. Ponce, H. Silva, B. Ruffmann, K. Schulte, J. Membr. Sci. 254 (2005) 139.
[43] C.C. Yang, J. Power Sources 109 (2002) 22.
[44] C.C. Yang, S.J. Lin, J. Power Sources 112 (2002) 497.
[45] C.C. Yang, S.J. Lin, Mater. Lett. 57 (2002) 873.
[46] C.C. Yang, S.J. Lin, J. Appl. Electrochem. 33 (2003) 777.
[47] G.M. Wu, S.J. Lin, C.C. Yang, J. Membr. Sci. 275 (2006) 127.
[48] C.C. Yang, S.J. Lin, G.M. Wu, Mater. Chem. Phys. 92 (2005) 251.
[49] C.C. Yang, J. Membr. Sci. 288 (2007) 51.
[50] E.H. Yu, K. Scott, J. Power Sources 137 (2004) 248.
[51] E.H. Yu, K. Scott, Electrochem. Commun. 6 (2004) 361.
[52] E.H. Yu, K. Scott, R.W. Reeve, J. Electroanal. Chem. 571 (2003) 17.
[53] J.W. Rhim, H.B. Park, C.S. Lee, J.H. Jun, D.S. Kim, Y.M. Lee, J. Membr. Sci. 238 (2004) 143.
[54] C.W. Lin, R. Thangamuthu, C.J. Yang, J. Membr. Sci. 253 (2005) 23.
[55] J.R. Varcoe, R.C.T. Slade, Electrochem. Commun. 8 (2006) 839.
[56] J.R. Varcoe, R.C.T. Slade, E.L.H. Yee, Chem. Commun. (2006) 1428.
[57] R. Varcoe, R.C.T. Slade, Fuel Cells 5 (2005) 187.
[58] T.N. Danks, R.C.T. Slade, J.R. Varcoe, J. Mater. Chem. 12 (2002) 3371.
[59] C.C. Yang, Int. J. Hydrogen Energy 29 (2004) 135.
[60] C.C. Yang, S.T. Hsu, W.C. Chien, M.C. Shih, S.J. Chiu, K.T. Lee, C.L. Wang, Int. J. Hydrogen Energy 31 (2006) 2076.
[61] A. Martinelli, A. Matic, P. Jacobsson, L. Borjesson, M.A. Navarra, A. Fernicola, S. Panero, B. Scrosati, Solid State Ionics 177 (2006) 2431.
[62] J.W. Kim, K.S. Ji, J.P. Lee, J.W. Park, J. Power Sources 119–121 (2003) 415.